

Multiple-frequency distorted-wave Born approach to 2D inverse profiling

Anton G Tjihuis¹, Kamal Belkebir^{2,4}, Amélie C S Litman³ and Bastiaan P de Hon¹

¹ Faculty of Electrical Engineering, Eindhoven University of Technology, PO Box 513, 5600 MB Eindhoven, The Netherlands

² Institut Fresnel, UMR-CNRS 6133, Campus de Saint Jérôme, case 162, 13397 Marseille Cedex 20, France

³ Schlumberger Riboud Production Center, 26 rue de la Cavee, BP 202, 92142 Clamart Cedex, France

E-mail: kamal.belkebir@fresnel.fr

Received 23 April 2001, in final form 20 July 2001

Published 13 November 2001

Online at stacks.iop.org/IP/17/1635

Abstract

The present paper deals with the inversion from experimental data provided by Institut Fresnel, France. The distorted-wave Born iterative approach is applied to the reconstruction of two lossless configurations involving dielectric circular cylinders. The dynamic range and the resolution of this scheme are governed by the operating frequency. For a low frequency, the dynamic range is large and the resolution is limited; raising the frequency improves the resolution at the cost of dynamic range. To obtain a high resolution for a large contrast, scattered-field information at multiple frequencies can be used. This is demonstrated for two cases where a direct inversion does not lead to convergence.

(Some figures in this article are in colour only in the electronic version)

1. Introduction

Inverse-profiling problems are traditionally expressed as optimization problems, in which the unknown configuration is parametrized and the value of the configuration parameters is determined by minimizing some cost function involving the scattered field. This is realized by iterative procedures based on a linearization around a given estimate, or by nonlinear optimization. The main bottleneck in solving multi-dimensional inverse-scattering problems in this manner is that repeated ‘exact’ field computations require an excessive amount of computation time. Combining the CGFFT (conjugate gradient fast Fourier transform) method with a special extrapolation procedure as described in [1, 2] can provide the required acceleration of these computations. Thus, field problems can be solved for a varying physical parameter by ‘marching on’ in that parameter.

⁴ To whom correspondence should be addressed.

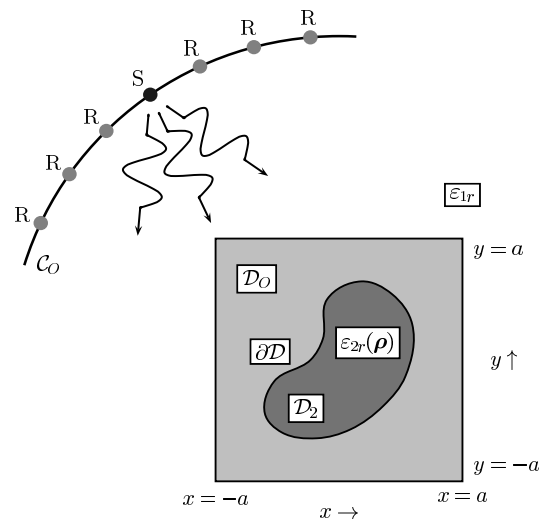


Figure 1. The dielectric cylinder, part of the observation contour and the various domains mentioned in the text. The region \mathcal{D}_1 is the region outside $\partial\mathcal{D}$.

The second issue is convergence. For linearized methods, convergence is not always guaranteed. Methods based on the optimization of a cost function inherently converge to a minimum, but this may be a local one. In the present paper, we demonstrate one way of avoiding this problem. We use the distorted-wave Born iterative procedure, which is one of the simplest linearized schemes. Results obtained by linearized techniques have been available in the open literature for some time [3–6]. However, most of the early work amounts to computational ‘trial and error’. A theoretical analysis was summarized in [7–10], but was only recently described in detail in [11]. In that paper, the distorted-wave Born iterative procedure is analysed from a theoretical and computational point of view. Based on an investigation of resolution and dynamic range, it is argued that configurations with a large contrast with respect to the surrounding medium can be reconstructed with an acceptable resolution by using multiple-frequency information. This is illustrated by representative numerical results for synthetic data. A similar conclusion was also reached in [12] and [13]. A second result from the theoretical analysis is the parametrization of the unknown susceptibility profile.

In [11], the approach was illustrated with the aid of representative numerical results. In the present paper, we describe its validation from real data. As in [11], we restrict ourselves in the examples to lossless dielectric objects. This allows us to avoid discussion of the frequency dependence of a complex permittivity. However, the algorithm is applicable to lossy objects as well.

2. Distorted-wave Born method

In this section, we specify the configuration and summarize the method of solution.

2.1. Formulation of the problem

We consider a two-dimensionally inhomogeneous, isotropic dielectric cylinder in a homogeneous surrounding medium. As shown in figure 1, the interior of the cylinder is represented as \mathcal{D}_2 , the boundary as $\partial\mathcal{D}$ and the exterior as \mathcal{D}_1 . For the permittivity, we have

$\varepsilon = \varepsilon_2(\boldsymbol{\rho})$ in \mathcal{D}_2 and $\varepsilon = \varepsilon_1$ in \mathcal{D}_1 , while the permeability $\mu = \mu_0$ in $\mathcal{D}_1 \cup \mathcal{D}_2$. We assume that the cylinder is enclosed in a square domain \mathcal{D}_O of width $2a$ centred around the z axis. The configuration is excited by an electrically polarized, time-harmonic line source which is located on a circular observation contour \mathcal{C}_O , with $\rho = \rho_O$. The electric field is detected by receivers on the same contour. A time factor of $\exp(st)$ with $s = \beta + j\omega$ is assumed implicitly.

2.2. Basic relations

Since the forward problem is linear, it suffices to consider the Green's function, i.e. the solution of the second-order differential equation

$$\left[\nabla_T^2 - \frac{s^2}{c_0^2} \varepsilon_r(\boldsymbol{\rho}) \right] G(\boldsymbol{\rho}, \boldsymbol{\rho}_P) = -\delta(\boldsymbol{\rho} - \boldsymbol{\rho}_P) \quad (1)$$

that satisfies the radiation condition

$$\lim_{\rho \rightarrow \infty} \sqrt{\rho} \left[\partial_\rho G(\boldsymbol{\rho}, \boldsymbol{\rho}_P) + \frac{s}{c_1} G(\boldsymbol{\rho}, \boldsymbol{\rho}_P) \right] = 0. \quad (2)$$

In (1) and (2), $\boldsymbol{\rho}$ and $\boldsymbol{\rho}_P$ are two-dimensional position vectors, ∇_T is the two-dimensional gradient operation, c_0 is the speed of light in free space, c_1 is the complex wave speed in \mathcal{D}_1 , ε_r is a complex relative permittivity and $\delta(\boldsymbol{\rho})$ is a two-dimensional delta function. Equation (1) is valid for all $\boldsymbol{\rho} \in \mathbb{R}^2$, with $\varepsilon_r(\boldsymbol{\rho}) = \varepsilon_{1r}$ for $\boldsymbol{\rho} \in \mathcal{D}_1$. With the aid of the radiation condition (2) and Green's second identity, it can be shown directly that G satisfies the reciprocity relation $G(\boldsymbol{\rho}_P, \boldsymbol{\rho}_Q) = G(\boldsymbol{\rho}_Q, \boldsymbol{\rho}_P)$ for any pair $\{\boldsymbol{\rho}_P, \boldsymbol{\rho}_Q\}$ in \mathbb{R}^2 .

Equation (1) can be reduced to an equivalent integral relation. We introduce a reference medium with relative permittivity $\bar{\varepsilon}_r(\boldsymbol{\rho})$ and the corresponding Green's function $\bar{G}(\boldsymbol{\rho}, \boldsymbol{\rho}_P)$. In principle $\bar{\varepsilon}_r(\boldsymbol{\rho})$ may be chosen arbitrarily; in the present context we will assume that this parameter only differs from ε_{1r} inside \mathcal{D}_O . Subtracting the differential equations for G and \bar{G} , writing the contrast source as a superposition of delta functions, and using reciprocity for \bar{G} results in the contrast-type integral relation

$$G(\boldsymbol{\rho}, \boldsymbol{\rho}_P) - \bar{G}(\boldsymbol{\rho}, \boldsymbol{\rho}_P) = -\frac{s^2}{c_0^2} \iint_{\mathcal{D}_O} [\varepsilon_r(\boldsymbol{\rho}') - \bar{\varepsilon}_r(\boldsymbol{\rho}')] \bar{G}(\boldsymbol{\rho}', \boldsymbol{\rho}) G(\boldsymbol{\rho}', \boldsymbol{\rho}_P) dA(\boldsymbol{\rho}') \quad (3)$$

which again holds for any pair $\{\boldsymbol{\rho}, \boldsymbol{\rho}_P\}$ in \mathbb{R}^2 .

2.3. Distorted-wave Born iterative procedure

In the inversion, we introduce a parametrization for the unknown profile by writing the relative permittivity as

$$\tilde{\varepsilon}_r(\boldsymbol{\rho}) = \varepsilon_{1r} + \tilde{\chi}(\boldsymbol{\rho}) = \varepsilon_{1r} + \sum_{\alpha} \tilde{\chi}_{\alpha} \psi_{\alpha}(\boldsymbol{\rho}) \quad (4)$$

where $\{\psi_{\alpha}(\boldsymbol{\rho})\}$ is a finite set of known, real-valued expansion functions with support inside the observation domain \mathcal{D}_O . The expansion parameters $\{\tilde{\chi}_{\alpha}\}$ are the fundamental unknowns in our numerical procedure.

The integral relation (3) is used in two ways in the reconstruction of $\varepsilon_r(\boldsymbol{\rho})$. In each iteration step, we start from a previously estimated permittivity profile $\tilde{\varepsilon}_r^{(n-1)}(\boldsymbol{\rho})$ of the form (4). For sources at $\boldsymbol{\rho}_P \in \mathcal{C}_O$, we determine the fields $\tilde{G}^{(n-1)}(\boldsymbol{\rho}, \boldsymbol{\rho}_P)$ that would be present in \mathcal{D}_O in this configuration. In (3), we choose $\varepsilon_r(\boldsymbol{\rho}) = \tilde{\varepsilon}_r^{(n-1)}(\boldsymbol{\rho})$, $\bar{\varepsilon}_r(\boldsymbol{\rho}) = \varepsilon_{1r}$ and $\boldsymbol{\rho} \in \mathcal{D}_O$. This results in the integral equation

$$\tilde{G}^{(n-1)}(\boldsymbol{\rho}, \boldsymbol{\rho}_P) = G_1(\boldsymbol{\rho}, \boldsymbol{\rho}_P) - \frac{s^2}{c_0^2} \iint_{\mathcal{D}_O} \tilde{\chi}^{(n-1)}(\boldsymbol{\rho}') G_1(\boldsymbol{\rho}, \boldsymbol{\rho}') \tilde{G}^{(n-1)}(\boldsymbol{\rho}', \boldsymbol{\rho}_P) dA(\boldsymbol{\rho}'). \quad (5)$$

In (5), $G_1(\boldsymbol{\rho}, \boldsymbol{\rho}') = \frac{1}{2\pi} K_0(\frac{s}{c_1} |\boldsymbol{\rho} - \boldsymbol{\rho}'|)$, with K_0 the modified Bessel function of the second kind of order zero, is the Green's function of the surrounding medium.

In the numerical solution of (5), we use the space discretization described in [2]. This discretization preserves the convolution-type structure of (5), and is second-order accurate in the mesh size $h = 2a/N$, with N the number of cells in the x and y directions. The equation is solved by the CGFFT method. The initial estimate is obtained by taking a linear combination of previous 'final' solutions and determining the coefficients by minimizing the squared error in the equality from (5) for the problem at hand. For $n = 1, 2$, we march on in angle, i.e. we generate the initial estimates for the CGFFT method from the fields for the same profile estimate for previous source positions. For $n \geq 3$, we march in contrast, i.e. we use the field for the correct source position for previous profile estimates.

Next, we determine the 'profile update'. The integral relation (5) for $\boldsymbol{\rho} = \boldsymbol{\rho}_R$ and $\boldsymbol{\rho}_P = \boldsymbol{\rho}_S$ is used to obtain the distorted-wave Born approximation for the field on \mathcal{C}_O . This results in

$$G(\boldsymbol{\rho}_R, \boldsymbol{\rho}_S) - \tilde{G}^{(n-1)}(\boldsymbol{\rho}_R, \boldsymbol{\rho}_S) = -\frac{s^2}{c_0^2} \iint_{\mathcal{D}_O} \sum_{\alpha} [\tilde{\chi}_{\alpha}^{(n)} - \tilde{\chi}_{\alpha}^{(n-1)}] \psi_{\alpha}(\boldsymbol{\rho}) \tilde{G}^{(n-1)}(\boldsymbol{\rho}, \boldsymbol{\rho}_R) \tilde{G}^{(n-1)}(\boldsymbol{\rho}, \boldsymbol{\rho}_S) dA(\boldsymbol{\rho}). \quad (6)$$

In this equation the 'profile update', represented by the coefficients $\{\tilde{\chi}_{\alpha}^{(n)} - \tilde{\chi}_{\alpha}^{(n-1)}\}$, is determined by minimizing the integrated squared error in the equality sign in (6).

In our implementation, the parametrization of the contrast function $\tilde{\chi}(\boldsymbol{\rho})$ in (4) is chosen such that this function is approximated by a piecewise bilinear expansion in $-a < x < a$ and $-a < y < a$ on K^2 squares of width Mh . This means that the fields are computed on an M times finer mesh than the corresponding profile estimates. Thus we may compute the Green's functions $\tilde{G}^{(n-1)}(\boldsymbol{\rho}, \boldsymbol{\rho}_P)$ with $\boldsymbol{\rho} \in \mathcal{D}_O$ and $\boldsymbol{\rho}_P \in \mathcal{C}_O$ with sufficient accuracy, without increasing the number of unknown profile parameters.

2.4. Multiple frequencies

The formulation of the iterative procedure in section 2.3 leaves us with two fundamental questions: will the scheme converge and what resolution can we expect upon convergence? Both questions are discussed in detail in [11]. Whether convergence is achieved depends critically on the quality of the distorted-wave Born approximation in the first iteration step. A parameter study for a canonical problem indicates that the dynamic range of the Born-type iterative procedure is determined by $\omega \|\varepsilon_r - \varepsilon_r^{(0)}\|$, where $\|\cdot\|$ is the L_1 norm.

The second question is: how much information can be retrieved from the linearized equation? To obtain a feeling for this, we assume that the reference profile $\bar{\varepsilon}_r(\boldsymbol{\rho})$ is a smooth estimate of the actual profile $\varepsilon_r(\boldsymbol{\rho})$, and that the difference between both profiles is so small that the distorted-wave Born approximation is almost exact. Because of the linearity of (6), it then suffices to consider the reconstruction of a 'pixel', i.e. a deviation localized around a point $\boldsymbol{\rho} = \boldsymbol{\rho}_O$. An argument inspired by [14] and by the back-propagation algorithm from geophysical imaging then leads to the usual concept of a point-spread function, but this function now depends on ω and the local value $\bar{\varepsilon}_r(\boldsymbol{\rho}_O)$.

These results give rise to the following conclusions. Ideally, any reconstruction procedure should be started from a homogeneous space, i.e. from $\varepsilon_r^{(0)}(\boldsymbol{\rho}) = \varepsilon_{1r}$. In that case, the only *a priori* knowledge is the fact that the scatterer is located in \mathcal{D}_O . However, especially for large contrasts, this imposes a restriction on the maximum value of ω . This restriction, in turn, limits the resolution with which $\varepsilon_{2r}(\boldsymbol{\rho})$ is reconstructed upon convergence. To circumvent this problem, we use multiple frequencies. The first approximation of the unknown permittivity

profile is indeed obtained starting from $\varepsilon_r^{(0)}(\rho) = \varepsilon_{1r}$. This approximation is used as a starting value for a reconstruction at a larger value of ω . By gradually increasing the operating frequency, we are then able to determine the required detail of the configuration, even for large contrasts in permittivity between the cylinder and the surrounding free space.

For a complex permittivity, increasing the frequency implies a scaling of at least the imaginary part of $\varepsilon_{2r}(\rho)$ for a small enough frequency ω . Usually, the assumption of a Maxwellian model suffices. In the results presented in [11] and the present paper, our main intention was to demonstrate ‘proof of concept’. Therefore, we avoid this discussion and restrict ourselves to a lossless configuration. However, all programs are capable of handling lossy media.

2.5. Regularization

Finally, the resolution analysis described above leads to the conclusion that the amount of information that can be obtained may depend on the position ρ_O . In the piecewise bilinear representation (4), we use a uniform sampling of $\tilde{\chi}(\rho)$. This leaves us with two options for the choice of number of subintervals K . Either we can choose K so small that the problem is resolved for all ρ , or we can choose K so large that the available information can always be handled. In the first case, the unknown profile is locally undersampled where the local refractive index is large; in the second case, the profile is locally oversampled where this index is small. In our implementation, we have chosen the latter option. The resulting ambiguity is removed by augmenting the integrated squared error in the equality sign in (6) with the regularization term

$$\delta \left(\frac{K}{2a \rho_O} \right)^2 \left\{ \sum_{k=1}^{K-1} \sum_{\ell=0}^K |\tilde{\chi}_{k-1,\ell} - 2\tilde{\chi}_{k,\ell} + \tilde{\chi}_{k+1,\ell}|^2 + \sum_{k=0}^K \sum_{\ell=1}^{K-1} |\tilde{\chi}_{k,\ell-1} - 2\tilde{\chi}_{k,\ell} + \tilde{\chi}_{k,\ell+1}|^2 \right\} \quad (7)$$

where $\tilde{\chi}_{k,\ell}$ is the sampled susceptibility, and δ is a small parameter. The terms in (7) restrict the variation in derivative in the x and y directions between adjacent cells. Our version of regularization does not add new information, but merely results in an ‘adaptive’ sampling. The normalization of the constant in (7) is chosen such that the smoothing effect remains invariant in a multi-grid reconstruction. Finally, the regularization term in (7) involves the total susceptibility, and not the profile update. Particularly in the presence of noise, this choice avoids a possible dependence of the final result on the initial estimate.

3. Numerical results

3.1. General considerations

Results of the reconstruction of two-dimensional dielectric objects from experimental data are reported in the present section. As mentioned above, we restrict ourselves to the reconstruction of lossless dielectric cylinders. The data were provided courtesy of Institut Fresnel, Marseille, France. The experimental setup as well as the database are described in the introduction to the special section. Two sets are used: the first one (filename: dielTM_dec8f.exp) concerns an off-centred circular dielectric of permittivity $\varepsilon_{2r} = 3$, and the second set (filename: twodielTM_8f.exp) deals with two identical circular dielectric cylinders, both with $\varepsilon_{2r} = 3$. For the circle along which the sources and the receivers are located, we took the radius $\rho_O = \rho_S = \rho_R \approx 74$ cm in both cases. In the inversion algorithm we modelled the incident field in the scattering domain G^{inc} as an electrically polarized field generated by a line source

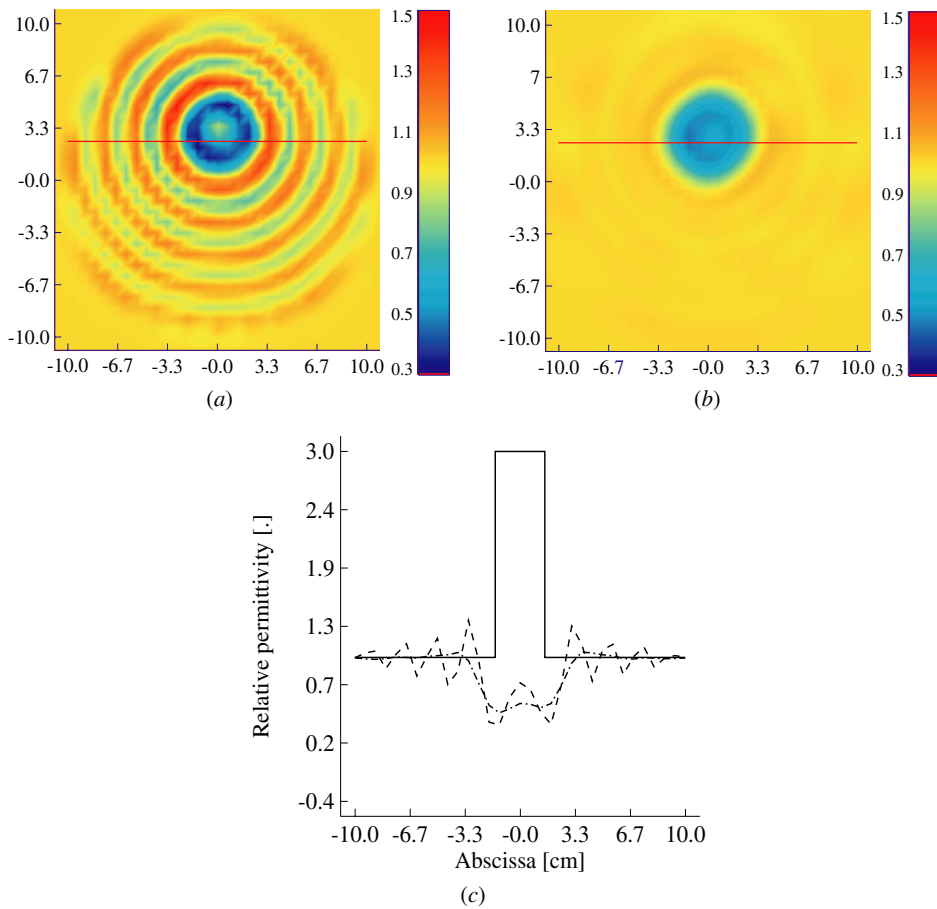


Figure 2. Reconstructed relative permittivity profile of the single dielectric cylinder at $f = 8$ GHz with two different values of the regularization parameter and comparison between the reconstructed profiles and the actual one. $N = 64$ and $K = 32$. (a) $\delta = 10^{-9}$ for $n = 1, 2$ and $\delta = 10^{-10}$ for $n \geq 3$; (b) $\delta = 10^{-7}$ for $n = 1, 2$ and $\delta = 10^{-8}$ for $n \geq 3$; (c) cross section along the line $y = 2.5$ cm; — actual profile, - - - reconstructed permittivity in (a), — · — reconstructed permittivity in (b).

weighted by a complex number γ . The frequency-dependent weight is determined by looking at the measured incident field when the receiving antenna lies opposite the emitting one:

$$G^{\text{inc}}(\rho_R, \rho_S) = \gamma G_1(\rho_R, \rho_S), \quad \gamma = \frac{2\pi G_{\text{mes}}^{\text{inc}}(\theta_S = 0, \theta_R = \pi)}{K_0(2\frac{s}{c_1}\rho_O)} \quad (8)$$

where $G_{\text{mes}}^{\text{inc}}$ is the measured incident field. The observation domain \mathcal{D}_O used for the inversion is a large square of side size $2a = 20$ cm. In terms of wavelength in the material this means that $2a \approx 9\lambda$ at the highest frequency $f = 8$ GHz. All results presented in this section correspond to the tenth iteration.

3.2. Single-frequency inversion

To illustrate the need for the multiple-frequency approach we first try to invert directly for the single frequency $f = 8$ GHz. Figures 2 and 3 show the results of the inversion for the

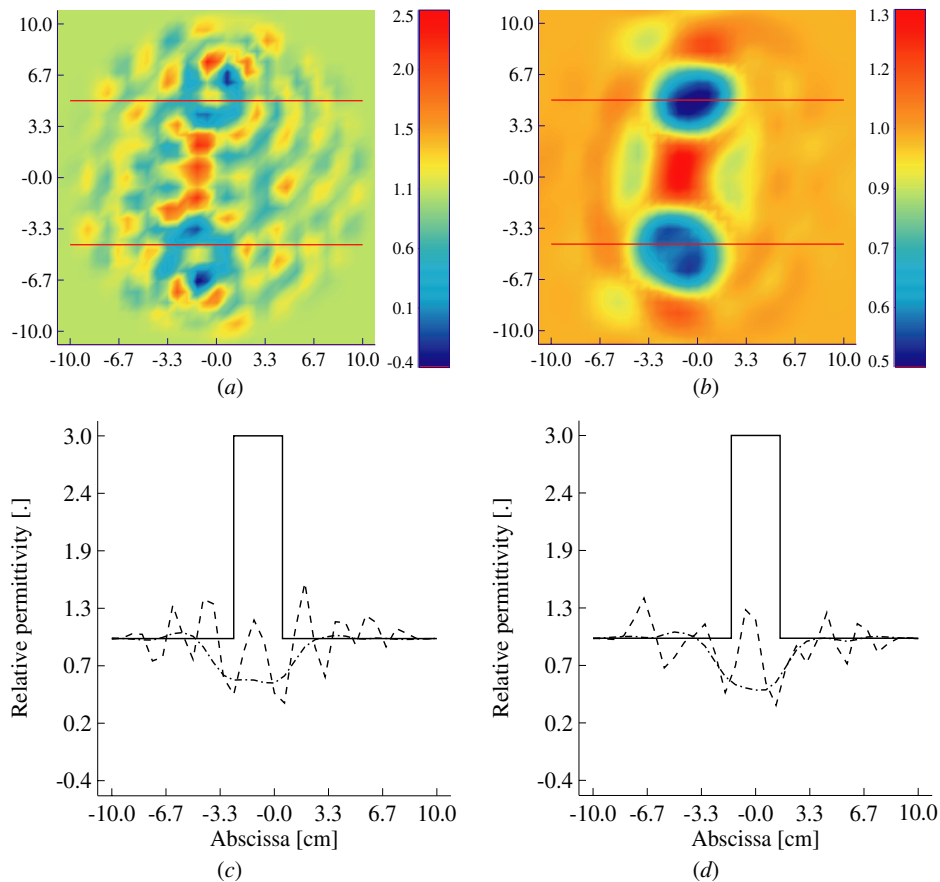


Figure 3. Reconstructed relative permittivity profile of two circular dielectric cylinders at $f = 8$ GHz with two different values of the regularization parameter. $N = 64$ and $K = 32$. (a) $\delta = 10^{-9}$ for $n = 1, 2$ and $\delta = 10^{-10}$ for $n \geq 3$; (b) $\delta = 10^{-7}$ for $n = 1, 2$ and $\delta = 10^{-8}$ for $n \geq 3$; (c) cross section along the line $y = -4.4$ cm (lower cylinder): — actual profile, - - - reconstructed permittivity in (a), - · - reconstructed permittivity in (b); (d) as in (c) for the upper cylinder, i.e. cross section along the line $y = 5$ cm.

single and the twin cylinders, respectively. It is observed that the scheme fails to retrieve the profiles, even when the value of the regularization parameter is increased. The regularization has a smoothing effect on the solution and leads to an acceptable reconstruction of the shape. However, the reconstructed permittivity does not have a physical meaning. From these results we conclude that for $f = 8$ GHz the distorted-wave Born scheme does not converge to the actual profiles if we start from $\varepsilon_{2r}(\rho) = \varepsilon_{1r} = 1$.

3.3. Using the multiple-frequency approach

We now apply the multiple-frequency approach for reconstructing the cylinders. We start with $f = 1$ GHz, use the final result as the initial guess for $f = 2$ GHz, and repeat this procedure for $f = 4$ and 8 GHz. Figures 4 and 5 present the results. In the multiple-frequency approach, the resolution improves gradually as predicted by theory and the converged results for $f = 8$ GHz are good approximations of the actual profiles.

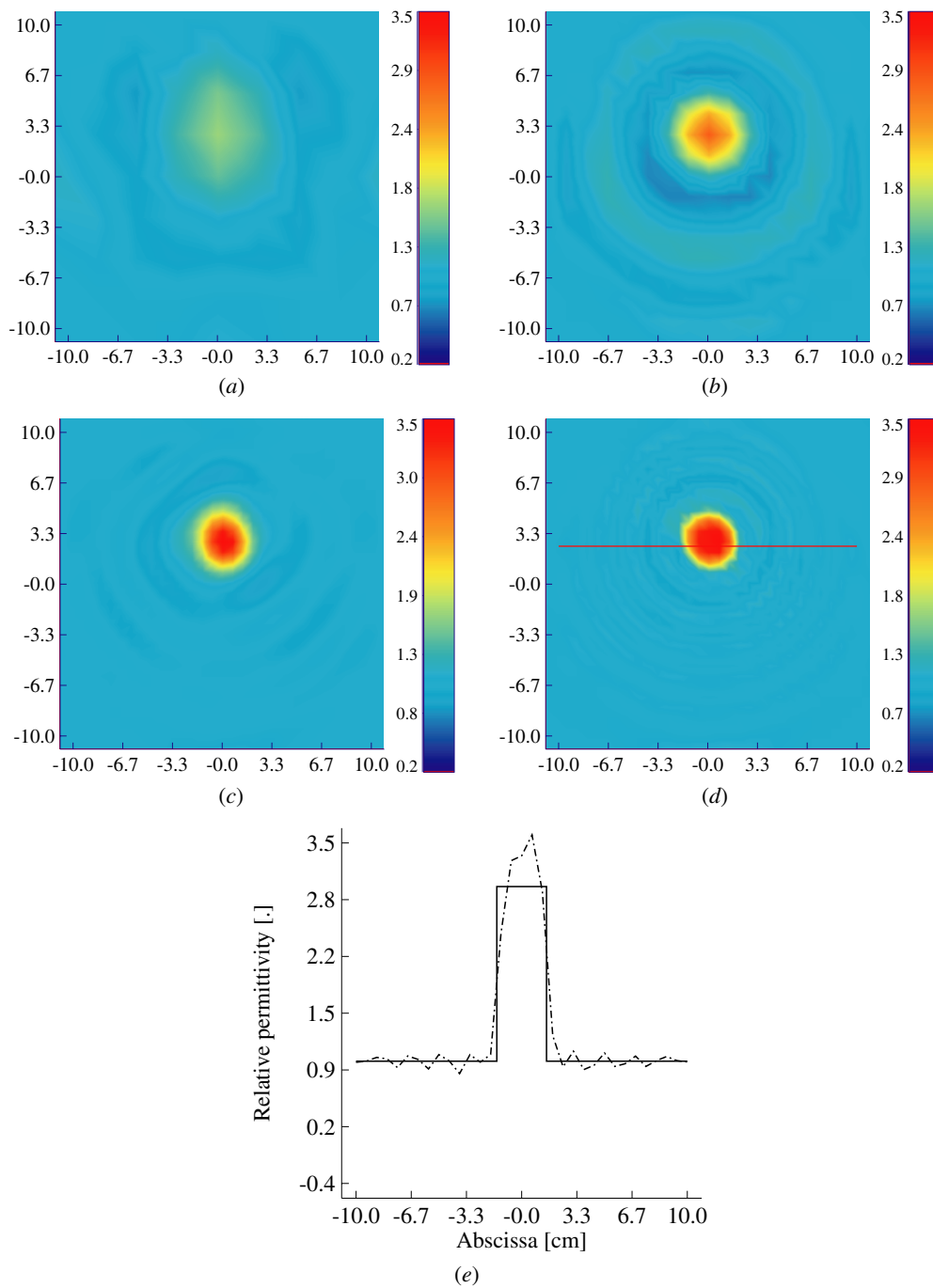


Figure 4. Reconstructed relative permittivity profile of the single dielectric cylinder at $f = 1$, 2, 4 and 8 GHz, respectively, using the multiple-frequency approach. (a) $f = 1$ GHz with $N = 8$ and $K = 8$; (b) $f = 2$ GHz with $N = 16$ and $K = 16$; (c) $f = 4$ GHz with $N = 32$ and $K = 32$; (d) $f = 8$ GHz with $N = 64$ and $K = 32$; (e) cross section along the line $y = 2.5$ cm plotted in (d): — actual profile, - - - reconstructed profile at $f = 8$ GHz. In all cases the regularization parameter is set to $\delta = 10^{-9}$ for $n = 1, 2$ and $\delta = 10^{-10}$ for $n \geq 3$.

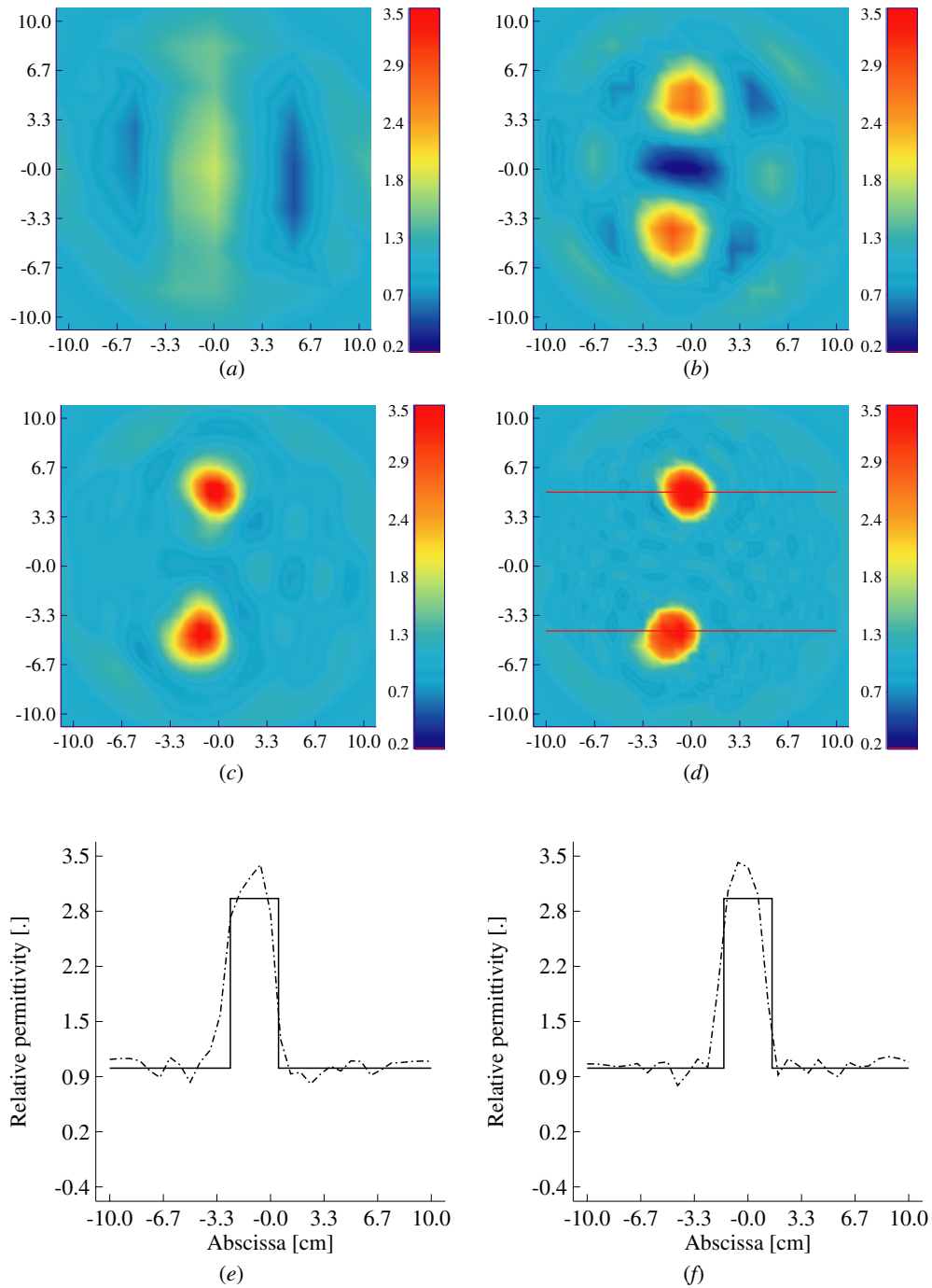


Figure 5. Reconstructed relative permittivity profile of the two identical circular dielectric cylinders at $f = 1, 2, 4$ and 8 GHz, respectively, using the multiple-frequency approach. (a) $f = 1$ GHz with $N = 8$ and $K = 8$; (b) $f = 2$ GHz with $N = 16$ and $K = 16$; (c) $f = 4$ GHz with $N = 32$ and $K = 32$; (d) $f = 8$ GHz with $N = 64$ and $K = 32$; (e) cross section along the line $y = -4.4$ cm plotted in (d): — actual profile, - - - reconstructed profile at $f = 8$ GHz; (f) as in (e) but for the upper cylinder ($y = 5$ cm). In all cases the regularization parameter is set to $\delta = 10^{-9}$ for $n = 1, 2$ and $\delta = 10^{-10}$ for $n \geq 3$.

4. Conclusion

When the successive approximate forward problems can be solved by a combination of the CGFFT method and ‘marching on in angle and/or contrast’, linearized schemes for profile inversion like the distorted-wave Born iterative procedure are capable of reconstructing 2D permittivity profiles from scattered-field data at a reasonable computational cost. However, the dynamic range of such schemes is limited by the operating frequency and the quality of the initial estimate. On the other hand, the resolution improves with increasing frequency. This suggests the use of multiple frequencies to obtain the required resolution in a number of steps. The theoretical justification of this idea has recently been described in detail in [11]. In the present paper, the ‘proof of the pudding’ for this idea was given by ‘eating’ real data. The configurations at hand could not be reconstructed directly from the data for $f = 8$ GHz. However, a very good reconstruction was obtained by ‘frequency hopping’ from $f = 1$ to 2, 4 and 8 GHz. Apart from a straightforward calibration procedure, no special care was needed in the algorithms described in [11]. With this result, linearized schemes are, in our opinion, a realistic alternative to the more involved, and therefore computationally more intensive, schemes.

References

- [1] Tjihuis A G and Peng Z Q 1991 Marching-on-in-frequency method for solving integral equations in transient electromagnetic scattering *IEE Proc. H* **138** 347–55
- [2] Peng Z Q and Tjihuis A G 1993 Transient scattering by a lossy dielectric cylinder: marching-on-in-frequency approach *J. Electromag. Waves Appl.* **7** 739–63
- [3] Wang Y M and Chew W C 1989 An iterative solution of two-dimensional electromagnetic inverse scattering problem *Int. J. Imag. Syst. Technol.* **1** 100–8
- [4] Chew W C and Wang Y M 1990 Reconstruction of two-dimensional permittivity distribution using the distorted wave Born iterative method *IEEE Trans. Med. Imaging* **9** 218–35
- [5] Moghaddam M and Chew W C 1992 Nonlinear two-dimensional velocity profile inversion in the time domain *IEEE Trans. Geosci. Remote Sens.* **30** 147–56
- [6] Joachimowicz N, Pichot Ch and Hugonin J-P 1991 Inverse scattering: an iterative numerical method for electromagnetic imaging *IEEE Trans. Antennas Propag.* **39** 1742–52
- [7] Tjihuis A G and Van Vliet F E 1993 Practical considerations for two-dimensional velocity inversion using the distorted-wave Born iterative technique *Proc. 24th General Assembly of URSI (Kyoto, Japan)* p 83
- [8] Tjihuis A G and Van Vliet F E 1994 Two-dimensional Born-type velocity inversion using multiple-frequency information *Proc. IEEE Antennas and Propagation Society Int. Symp. (Seattle, Washington)* pp 2288–91
- [9] Tjihuis A G and Van Vliet F E 1994 Two-dimensional Born-type velocity inversion using multiple-frequency information *Proc. PIERS Symp. (Noordwijk, the Netherlands)* p 404
- [10] Belkebir K and Tjihuis A G 1995 Using multiple frequency information in the iterative solution of a two-dimensional nonlinear inverse problem *Proc. PIERS Symp. (Innsbruck, Austria)* p 353
- [11] Tjihuis A G, Belkebir K, Litman A C S and De Hon B P 2001 Theoretical and computational aspects of two-dimensional inverse profiling *IEEE Trans. Geosci. Remote Sens.* **39** 1316–30
- [12] Chew W C and Lin J H 1995 A frequency-hopping approach for microwave imaging of large inhomogeneous bodies *IEEE Microw. Guided Wave Lett.* **15** 439–41
- [13] Chen Y 1997 Inverse scattering via Heisenberg’s uncertainty principle *Inverse Problems* **13** 253–82
- [14] Broquetas A, Mallorquí J J, Rius J M, Jofre L and Cardama A 1993 Active microwave sensing of highly contrasted dielectric bodies *J. Electromag. Waves Appl.* **7** 1439–53